Journal of Solid State Chemistry 221 (2015) 272–277

Contents lists available at ScienceDirect

Journal of Solid State Chemistry

journal homepage: www.elsevier.com/locate/jssc

Synthesis, structure and properties of layered iron-oxychalcogenides $Nd_2Fe_2Se_{2-x}S_xO_3$

Y. Liu [a], S.B. Zhang [a,*], S.G. Tan [a], B. Yuan [a], X.C. Kan [a], L. Zu [a], Y.P. Sun [a,b,c,**]

[a] Key Laboratory of Materials Physics, Institute of Solid State Physics, Chinese Academy of Sciences, Hefei 230031, People's Republic of China
[b] High Magnetic Field Laboratory, Chinese Academy of Sciences, Hefei 230031, People's Republic of China
[c] University of Science and Technology of China, Hefei 230026, People's Republic of China

ARTICLE INFO

Article history:
Received 29 May 2014
Received in revised form
3 September 2014
Accepted 11 September 2014
Available online 30 October 2014

Keywords:
Sulfur substitution
Semiconductor
Antiferromagnetic
Thermoelectric

ABSTRACT

A new series of sulfur-substituted iron-oxychalcogenides $Nd_2Fe_2Se_{2-x}S_xO_3$ ($0 \le x \le 0.4$) was synthesized by solid state reaction method, and investigated by structure, transport, magnetic and specific heat measurements. The compounds crystallize in the layered tetragonal structure with $I4/mmm$ space group, and show semiconducting behavior. The large discrepancy between the activation energies for conductivity, E_ρ (152–202 meV), and thermopower, E_S (15.6–39.8 meV), indicates the polaronic transport mechanism of the carrier. The parent compound $Nd_2Fe_2Se_2O_3$ exhibits a frustrated antiferromagnetic (AFM) ground state, and the S-substitution induces an enhanced ferromagnetic (FM) component and possible increased degree of frustration.

1. Introduction

Layered transition-metal compounds have been extensively studied for decades owing to their novel physical properties, especially colossal magnetoresistance in layered manganites [1,2], giant thermoelectric power in layered cobaltates [3–5], and high-T_c superconductivity in layered cuprates and iron-based superconductors [6–9].

Kamihara et al. reported superconductivity with $T_c=26$ K in $LaO_{1-x}F_xFeAs$ [10]. Later, in other F-doped *Ln*FeAsO (*Ln*=rare earth elements) compounds, the T_c increased rapidly, including $T_c=41$ K in $CeO_{1-x}F_xFeAs$ [7] and $T_c=52$ K in $PrO_{1-x}F_xFeAs$ [11], and reached $T_c=55$ K in $SmO_{1-x}F_xFeAs$ [12]. Besides the F-doping in O sites, the superconductivity could also be observed in *Ln*FeAsO via isovalent substitution of As by P [13]. Afterwards, the AFe_2As_2 (*A*=Ca, Sr, Ba, Eu) [9,14–18] and *A*FeAs (*A*=Li, Na) [19–21] type compounds were discovered. The superconductivity could be induced with $T_c=26$ K in $EuFe_2(As_{0.7}P_{0.3})_2$ [22] and $T_c=30$ K in $BaFe_2(As_{0.7}P_{0.3})_2$ [23], via partially substituting As by P. In Fe-chalcogenides, FeTe undergoes an antiferromagnetic (AFM) transition, which could be suppressed with partial substitution of Te by S or Se [24–26], and then, shows superconductivity. Therefore, the anion-substitution is an important method to investigate the physical properties by introducing chemical pressure or adjusting carrier content.

Recently, a series of $R_2Fe_2Se_2O_3$ (*R*=La–Sm) has gathered much attention, which shows a similar local environment of Fe ions to that in Fe-based superconductors [27–30]. Unfortunately, they show antiferromagnetic (AFM) semiconducting ground state. In this series, the R_2O_2 sheets of edge-sharing OR_4 tetrahedron alternate with Fe_2OSe_2 layers of face-sharing octahedron. Within the Fe_2OSe_2 layer, the FeO_2Se_4 octahedrons are distorted due to different Fe–Se and Fe–O bond distances. There are three basic interactions: the nearest neighbor (*NN*) J_3 interaction of Fe–Fe, the next nearest neighbor (*NNN*) J_2 interaction of Fe–Se–Fe, and the *NNN* J_1 interaction of Fe–O–Fe. Theoretical calculation and neutron diffraction results indicate that the AFM transition stems from the competition of these three interactions in an unusual frustrated AFM checkerboard spin-lattice. The evolution of structure and magnetic properties tuned by Fe/Mn ratio in $La_2(Fe_{1-x}Mn_x)_2Se_2O_3$ was investigated, and shows a rich magnetic phase diagram [31]. So far, there is no report on the effect of anion-substitution in this system. As we discussed above, the anion-substitution plays an important role to adjust the ground state of the iron-based superconductors. Therefore, we try to study the anion-substitution effect in this system.

In this study, we successfully synthesized a new series of anion-substituted compounds $Nd_2Fe_2Se_{2-x}S_xO_3$ ($0 \le x \le 0.4$). Systematical measurements, including X-ray diffraction (XRD), electrical resistivity, thermoelectric power, magnetic susceptibility, and specific heat, were subsequently performed to shed light on the

* Corresponding author.
** Corresponding author at: Key Laboratory of Materials Physics, Institute of Solid State Physics, Chinese Academy of Sciences, Hefei 230031, People's Republic of China.
E-mail addresses: sbzhang@issp.ac.cn (S.B. Zhang), ypsun@issp.ac.cn (Y.P. Sun).

http://dx.doi.org/10.1016/j.jssc.2014.09.038
0022-4596/

physical properties, and the anion sulfur substituted effect was discussed.

2. Experimental

$Nd_2Fe_2Se_{2-x}S_xO_3$ ($0 \leq x \leq 0.4$) polycrystals were synthesized by solid state reaction method using Nd_2O_3 (99.99%), Fe (99.9%), Se (99.95%), and S (99.9%) powder as raw materials. Nd_2O_3 was dried by heating in air at 1173 K for 20 h before using. The powder was weighed according to the stoichiometric ratio, thoroughly grounded, pressed into a pellet and then sealed in an evacuated quartz tube ($<10^{-3}$ Pa). The tube was heated to 1273 K and reacted for 24 h followed by furnace cooling. The process was repeated twice to ensure homogeneity. The powder XRD was performed using a Philips X'Pert PRO X-ray diffractometer with Cu $K\alpha$ radiation ($\lambda=1.54$ Å). The structural parameters were obtained by using the Rietveld method with the X'Pert Plus software. Transport, specific heat and magnetic measurements were carried out in Quantum Design PPMS-9 and MPMS-5 system, respectively.

3. Results and discussion

3.1. Structure

Fig. 1(a) shows the crystal structure of $Nd_2Fe_2Se_{2-x}S_xO_3$ ($0 \leq x \leq 0.4$), which is built up by stacking fluorite-like Nd_2O_2 layers and $Fe_2O(Se/S)_2$ layers alternatively along the c axis. The Fe_2O sheets adopt an unusual anti-CuO_2 arrangement with Fe^{2+} cations coordinated by two in-plane O^{2-} and four Se^{2-} above and below the plane, leading to face-shared FeO_2Se_4 octahedron. Fig. 1 (b) shows the powder XRD patterns for $Nd_2Fe_2Se_{2-x}S_xO_3$ ($0 \leq x \leq 0.4$), scanning over a 2θ range of 20°–80° at room temperature. The refinement curves are obtained by the Rietveld method with the X'Pert Plus software. All the reflections could be indexed with
$I4/mmm$ space group and the structure details are summarized in Table 1. With increasing x, the diffraction peaks gradually shift to higher angle degree, which is illustrated by the enlargement of peak (1 1 2) shown in the inset of Fig. 1(b), indicating a contraction of the lattice. It is mainly due to the smaller radius of S than that of Se atom. Fig. 1(c) shows the evolution of the lattice parameters ($a=b$, c) and unit cell volume (V), which shows approximately linear x-dependence, indicating the well substitution in Se(S) sites. The lattice parameters of $x=0$ ($a=4.0231(4)$ Å and $c=18.456(2)$ Å) gradually decrease to those of $x=0.4$ ($a=4.0130(5)$ Å and $c=18.310(2)$ Å). The unit cell volume (V) variation ($\delta=(V_{x=0}-V_{x=0.4})/V_{x=0}$) is about 1.29%.

Fig. 2(a) depicts the $Fe_2O(Se/S)_2$ layer from a vertical view with Se/S atoms puckering above and below the square Fe_2O sheet. The evolution of the nearest intralayer Fe–Fe distance (d_{Fe-Fe}), together with the Fe–O and Fe–Se/S bond distances (d_{Fe-O} and $d_{Fe-Se/S}$), is shown in Fig. 2(b). All the distances decrease with increasing x. For $Nd_2Fe_2Se_2O_3$ ($x=0$), the approximated bond-valence-sum (BVS) of Fe ion has been calculated as +2.02 using the equation of $BVS=\sum\exp[(R-d)/0.37]$, where R is the bond valence parameter and d is the bond length [32,33]. The calculated result is rather close the expected value and confirms the existence of Fe^{2+} ionic state. In addition, we calculated the ratio of d_{Fe-Fe}:$d_{Fe-Se/S}$ and it increases from 1.047 for $x=0$ to 1.050 for $x=0.4$. Fig. 2(c) shows the local environment of each Fe^{2+} ion, which is a distorted octahedron due to different bond distances of d_{Fe-O} and $d_{Fe-Se/S}$. The bond angles of $\alpha_{Se/S-Fe-Se/S}$ are shown in Fig. 2(d). The ratio of $\alpha_{1(Se/S-Fe-Se/S)}$:$\alpha_{2(Se/S-Fe-Se/S)}$ gradually increases from 1.13 for $x=0$ to 1.14 for $x=0.4$, suggesting the S-doping in Se sites slightly enhances the degree of octahedral distortion.

3.2. Transport properties

Fig. 3 shows the temperature-dependent electrical resistivity (ρ) for $Nd_2Fe_2Se_{2-x}S_xO_3$ ($x=0$, 0.2, 0.4), which displays an obvious semiconducting behavior. The series of $A_2F_2Fe_2OQ_2$ (A=Sr, Ba; Q=S, Se) is Mott insulator with narrowing 3d electronic band due to strong correlation effect [34]. Considering the similar local environment of Fe^{2+} ions, $Nd_2Fe_2Se_{2-x}S_xO_3$ could also be regarded as correlation-induced semiconductor. Generally, there are mainly three models to well describe the semiconducting behavior. (1) the thermally activated model: $\rho(T)=\rho_0\exp(E/k_BT)$, where ρ_0 is the prefactor, E is the activation energy and k_B is Boltzmann constant. (2) the adiabatic small polaron hopping model: $\rho(T)=AT\exp(E_\rho/k_BT)$. (3) Mott's variable-range hopping (VRH) model: $\rho(T)=\rho_0\exp(T_0/T)^{1/3}$ for 2D system. Fig. 3 shows the fitting result of the adiabatic small polaron hopping model. The extracted activation energy E_ρ is shown in the inset of Fig. 3, which is about 152(5) meV for $x=0$, and gradually increase to 202

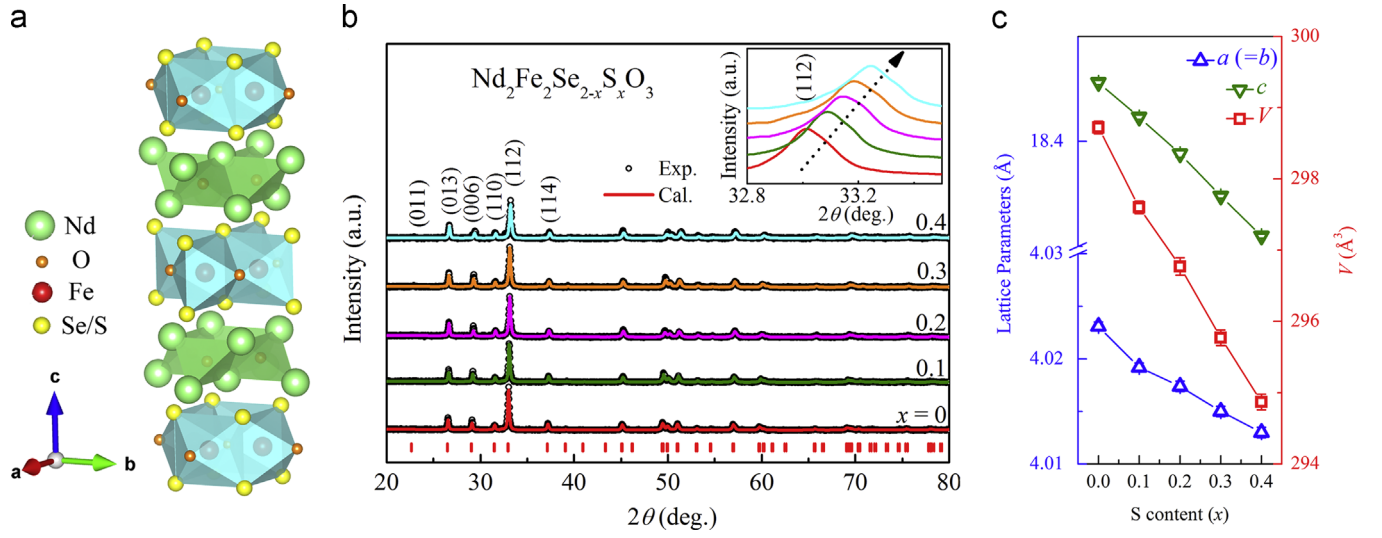

Fig. 1. (a) The crystal structure of $Nd_2Fe_2Se_{2-x}S_xO_3$ ($0 \leq x \leq 0.4$). (b) The powder XRD patterns together with the refinement curves. (c) The evolution of lattice parameters ($a=b$, c) and unit cell volume (V) with x.